

Cavity-Vacuum-Induced Chiral Spin Liquids in Kagome Lattices: Tuning and Probing Topological Quantum Phases via Cavity Quantum Electrodynamics

Chenan Wei,^{1, 2} Liu Yang,^{3, 4} and Qing-Dong Jiang^{3, 4, 5, *}

¹*Department of Physics, University of Massachusetts, Amherst, Massachusetts 01003, USA*

²*Department of Physics, University of Alberta, Edmonton, Alberta T6G 2E1, Canada*

³*Tsung-Dao Lee Institute, Shanghai Jiao Tong University, Shanghai 200240, China*

⁴*School of Physics and Astronomy, Shanghai Jiao Tong University, Shanghai 200240, China*

⁵*Shanghai Branch, Hefei National Laboratory, Shanghai 201315, China*

(Dated: November 14, 2024)

Topological phases in frustrated quantum magnetic systems have captivated researchers for decades, with the chiral spin liquid (CSL) standing out as one of the most compelling examples. Featured by long-range entanglement, topological order, and exotic fractional excitations, the CSL has inspired extensive exploration for practical realizations. In this work, we demonstrate that CSLs can emerge in a kagome lattice driven by vacuum quantum fluctuations within a single-mode chiral cavity. The chiral cavity imprints quantum fluctuations with time-reversal symmetry breaking, fostering chiral interactions among electrons and stabilizing a robust CSL phase without external laser excitation. Moreover, we identify experimentally accessible observables—such as average photon number and transport properties—that reveal connections between photon dynamics and the emergent chiral order. Our findings establish a novel pathway for creating, controlling, and probing topological and symmetry-breaking quantum phases in strongly correlated systems.

Introduction. Quantum spin liquids (QSLs) represent a unique class of “quantum disordered” ground states in spin systems, where strong zero-point fluctuations inhibit conventional magnetic long-range order. Among these, chiral spin liquids (CSLs) stand out as an intriguing subset characterized by broken time-reversal symmetry. CSLs have been extensively studied within strongly correlated systems for their potential to host topologically ordered states and exotic excitations, such as anyons—particles regarded as essential components for topological quantum computing [1–6]. Over the years, theoretical advances, including the study of moat bands and spontaneous chiral breaking in fermionic systems [7–17], have deepened our understanding of the fundamental mechanisms driving CSL formation. The chiral nature of these spin liquids may manifest through their response to probe electromagnetic field in both equilibrium and nonequilibrium settings [18], as well as through the emergence of circulating spin currents. These currents are often driven by geometric frustration in lattice structures, such as the kagome lattice, or by external perturbations like staggered magnetic fields or spin-orbit coupling.

The kagome lattice, with its corner-sharing triangular structure, is recognized as an ideal candidate for hosting CSL states due to its inherent geometric frustration. This frustration suppresses conventional magnetic ordering, fostering quantum fluctuations that stabilize exotic quantum phases such as spin liquids [19, 20]. Due to its unique geometric properties, the kagome lattice exhibits flat bands, Dirac cones, and a spin-liquid ground state, creating fertile ground for realizing topologically nontrivial phases [13, 21–24]. Recent theoretical and experimental studies on materials with kagome lattice structures have demonstrated QSL behavior, further supporting its suitability for realizing CSLs [25–27]. However, achieving

a chiral spin liquid phase requires additional mechanisms to break time-reversal symmetry and induce the chiral ordering needed for CSL formation [28, 29].

One promising approach for inducing the required chiral ordering is through cavity quantum electrodynamics (cQED). In cQED, strong electron-photon interactions within an optical cavity can significantly modify the properties of a material, leading to profound changes in its electronic, magnetic, topological and localization behavior [30–32]. By coupling quantum materials to cavity modes, researchers can dynamically tune the Hamiltonian, achieving precise control over quantum many-body systems, including QSLs [33].

In particular, in a chiral cavity, the polarization of the electromagnetic field can be engineered to break time-reversal symmetry, providing an additional handle to induce chiral symmetry breaking in quantum spin systems. This interaction with the quantum fluctuations in the cavity field could potentially induce topological order and stabilize chiral phases in systems that otherwise lack such behavior [34–46]. A straightforward method for making an effective chiral cavity involves utilizing a Faraday rotator (*e.g.*, ferromagnetic layer) in conjunction with high-quality metallic mirrors to establish a high-quality cavity [47–51].

In this work, we explore a novel mechanism for inducing CSL phases by coupling a kagome lattice to a chiral cavity (see fig. 1 for a schematic diagram of the setup). This setup leverages the interaction between virtual photons from vacuum fluctuations and electrons within the kagome lattice to dynamically break time-reversal symmetry and establish chiral order. The ability to control topological phases via a tunable cavity vacuum represents a remarkable alternative to prior studies on CSLs in strongly correlated systems. Specifically, we investi-

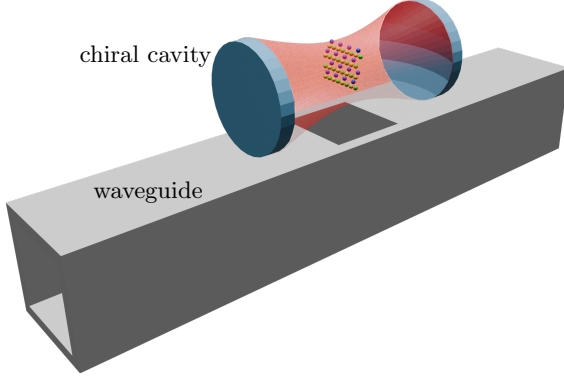


FIG. 1. The schematic diagram of the setup. The kagome lattice is placed inside a chiral cavity. The chiral cavity is coupled to a waveguide, which is used for transport measurement.

gate how coupling the lattice system to cavity modes can enhance quantum fluctuations and induce the chiral order needed for CSL phases. Furthermore, we propose experimentally accessible transport properties that link photon dynamics with the emergent chiral spin order. By examining the interplay between the frustrated kagome geometry and the electromagnetic quantum fluctuations within the cavity, we aim to provide a new avenue for engineering and probing topologically nontrivial order in frustrated magnetic systems.

Kagome lattice coupled to a chiral cavity. We start by exploring a single-particle model describing electrons in a kagome lattice coupled to a single-mode chiral cavity. The coupling of the cavity vacuum to electrons generates an effective gauge field, which plays a crucial role in forming a CSL state. Notably, this interaction is induced entirely by the vacuum fluctuations of the cavity, without requiring external laser driving. The full Hamiltonian is composed of three terms:

$$H = H_k + H_{cc} + V_{\text{lattice}} \quad (1)$$

where H_k describes the kinetic energy of electrons, H_{cc} represents the chiral cavity mode of energy ω_c , *i.e.*, $H_{cc} = \omega_c a^\dagger a$ with photon annihilation and creation operator a and a^\dagger , and V_{lattice} accounts for the potential energy from the kagome lattice. The kinetic energy Hamiltonian, incorporating the electromagnetic vector potential \mathbf{A} due to the cavity, is:

$$H_k = \frac{(\boldsymbol{\sigma} \cdot (\mathbf{p} - q\mathbf{A}))^2}{2m}, \quad (2)$$

where $\boldsymbol{\sigma}$ is the vector of Pauli matrices, \mathbf{p} is the momentum of the electrons, m is the mass of the electrons, the vector potential is $\mathbf{A} = A_0(\boldsymbol{\epsilon}a + \boldsymbol{\epsilon}^*a^\dagger)$ and, $\boldsymbol{\epsilon} = \frac{1}{\sqrt{2}}(1, i)$ represents circularly polarized mode due to the chiral cavity. Note that the Schrödinger-Pauli Hamiltonian (2) automatically incorporate the interaction of electron's

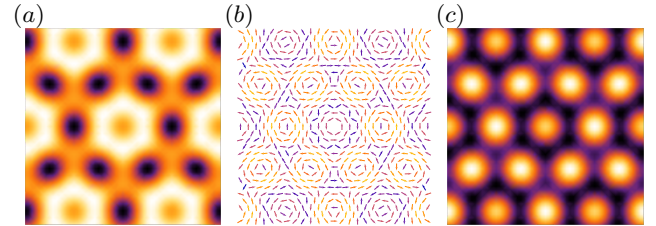


FIG. 2. (a) Kagome lattice potential from eq. (3). The dark dots are the low energy position, which form the kagome lattice. (b) The effective gauge vector potential \mathbf{A}_{eff} , the dark color being the stronger strength. (c) The gauge field flux $\nabla \times \mathbf{A}_{\text{eff}}$, which is a scalar in 2d.

spin with magnetic field. The kagome lattice potential can be approximated by [22]:

$$V_{\text{lattice}}(\mathbf{r}) = V_0[\phi(\mathbf{r}) - \phi(2\mathbf{r})], \quad (3)$$

where

$$\phi(\mathbf{r}) = \cos(\mathbf{b}_1 \cdot \mathbf{r}) + \cos(\mathbf{b}_2 \cdot \mathbf{r}) + \cos((\mathbf{b}_1 + \mathbf{b}_2) \cdot \mathbf{r}) \quad (4)$$

depends on the reciprocal vectors $\mathbf{b}_1 = \frac{4\pi}{\sqrt{3}}(\frac{\sqrt{3}}{2}, -\frac{1}{2})$, $\mathbf{b}_2 = \frac{4\pi}{\sqrt{3}}(0, 1)$. Such lattice potential is shown in fig. 2a. As will be shown later, the microscopic details of the lattice potential do not alter our results qualitatively.

Asymptotically decoupled frame. To study the impact of cavity quantum fluctuations on electronic system, we employ the asymptotically decoupled (AD) frame, a method originally used to study the cavity Lamb shift [52] and more recently highlighted for its significance in the study of cavity materials [53]. The AD frame is obtained by performing a unitary transformation that effectively decouples the cavity photons from the electronic degrees of freedom, which becomes exact at either the weak ($A_0 \ll 1$) or strong ($A_0 \gg 1$) coupling limits. This transformation is given by:

$$H_{\text{AD}} = U^\dagger H U; \quad \text{with } U = \exp(-i\xi \mathbf{p} \cdot \boldsymbol{\pi}) \quad (5)$$

where the parameter $\xi = \frac{qA_0}{m\tilde{\omega}_c}$ is of the length dimension, $\tilde{\omega}_c = \omega_c + \frac{q^2 A_0^2}{m}$, $\boldsymbol{\pi} = i(\boldsymbol{\epsilon}^* a^\dagger - \boldsymbol{\epsilon} a)$ represents the dimensionless photon field momentum.

In the AD frame, the Hamiltonian splits into two parts: one representing the electrons in an effective gauge field (noting that this effective gauge field is distinct from the photon field) and the other representing the photon field itself. Ultimately, we can derive a second-quantized lattice model that effectively describes the system. To ensure generality, we also incorporate the delta two-body interaction [54]

$$H_{\text{AD}} = - \sum_{\langle i,j \rangle, \sigma} t e^{i\varphi_{ij}} c_{i\sigma}^\dagger c_{j\sigma} + U' \sum_i n_{i\uparrow} n_{i\downarrow} + \sum_i \mathcal{B}(n_{i\uparrow} - n_{i\downarrow}) \quad (6)$$

a/nm	0.5	1
ϵ_r		
1	$L_c/a_0 = 222.4$ $V_0 = 70.9 \text{ eV}$	$L_c/a_0 = 111.2$ $V_0 = 17.7 \text{ eV}$
5	$L_c/a_0 = 99.5$ $V_0 = 14.2 \text{ eV}$	$L_c/a_0 = 49.8$ $V_0 = 3.6 \text{ eV}$
10	$L_c/a_0 = 70.3$ $V_0 = 7.1 \text{ eV}$	$L_c/a_0 = 35.2$ $V_0 = 1.8 \text{ eV}$

TABLE I. Cavity length L_c when the transition happens and the lattice potential V_0 needed to observe the CSL phase is shown for a range of parameters, namely lattice constant a_0 and the relative permittivity ϵ_r , when the cavity frequency $\omega_c = 2\pi \text{ THz}$.

where the phase factor $\varphi_{ij} = q \int_{\mathbf{r}_i}^{\mathbf{r}_j} \mathbf{A}_{\text{eff}} \cdot d\mathbf{r}$ and $\mathbf{A}_{\text{eff}} = \beta \hat{\mathbf{z}} \times \nabla[\phi(\mathbf{r}) - \phi(2\mathbf{r})]$ is the effective gauge field coupled to the electrons, with dimensionless strength $\beta = \frac{\tilde{m}\xi^2 V_0}{2}$ and $\tilde{m} = m + \frac{q^2 A_0^2}{\omega_c}$. In the last term, $\mathcal{B} = \frac{q^2 A_0^2}{2m}$ acts as an effective Zeeman splitting field.

By applying the AD unitary transformation and analyzing the resulting effective Hamiltonian, we observe how the coupling to a chiral cavity vacuum state introduces a nontrivial phase factor φ_{ij} in the electron hopping terms, the structure of which is shown in figs. 2b and 2c. This phase factor is crucial, as it breaks time-reversal symmetry and ultimately leads to the realization of a chiral spin liquid. We confirm this behavior through simulations using single-site density matrix renormalization group (DMRG) with subspace expansion [55]. The simulations are performed with 10×10 unit cells, and the results are shown in fig. 3. In fig. 3a, the chiral order $\bar{\chi} = \langle \mathbf{S}_i \cdot \mathbf{S}_j \times \mathbf{S}_k \rangle$ remains non-zero when the electron-photon coupling \mathcal{B} is smaller than a critical value. Beyond the critical value, the cavity quantum fluctuations (virtue photons) polarize the spin and the chiral order vanishes, which is reflected in the spin zz correlation G_{zz} in fig. 3b. By contrast, the zz correlation is close to zero for smaller photon-electron coupling \mathcal{B} . The absence of magnetic order and a non-zero chiral order confirms the CSL state of the system for weak photon-electron coupling. Our simulations show that chiral order is preserved for weak photon-electron coupling, while strong coupling suppresses this order and polarizes the spin.

In real situations, multiple electrons may coherently couple to a single cavity mode, resulting in a straightforward modification of parameters [54]

$$\begin{aligned} \tilde{\omega}_c &\rightarrow \tilde{\omega}_c^{(MB)} = \omega_c \left(1 + \frac{Nq^2 A_0^2}{m\omega_c}\right), \\ \tilde{m} &\rightarrow \tilde{m}^{(MB)} = m \left(1 + \frac{Nq^2 A_0^2}{m\omega_c}\right), \end{aligned} \quad (7)$$

where N is the number of total electrons. For the purpose of experimental observation, we estimate that the transition occurs around $A_0 \approx \frac{\sqrt{m\epsilon_r}}{q}$. It is important to note that the hopping parameter t implicitly depends on the cavity frequency as the chiral cavity renormalizes the

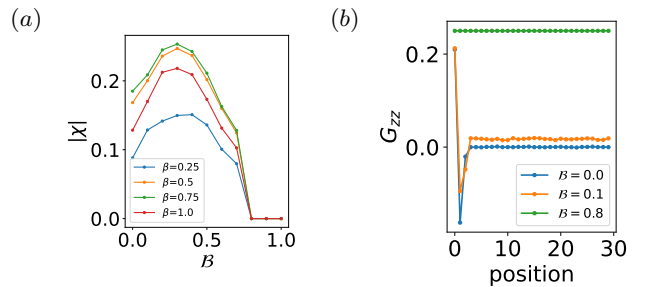


FIG. 3. Order parameters for the kagome lattice inside the chiral cavity. (a) is the chiral order parameter. DMRG simulation indicates non-zero chiral order parameter for weak electron-photon interaction and zero chiral order parameter for strong electron-photon interaction. $\beta = \frac{\tilde{m}\xi^2 V_0}{2}$ is the dimensionless parameter describing the strength of the effective gauge field. (b) is the spin zz correlation when $\beta = 0.5$. DMRG simulation indicates no or weak correlation for weak electron-photon interaction and strong correlation for strong electron-photon interaction. Combining with the nonzero chiral order in the weak-coupling regime, this confirms the presence of a CSL phase, while strong coupling leads to a spin-polarized state. All the simulations above are done with $t = 1$ and $U' = 5$.

mass to $\tilde{m}^{(MB)}$. Hence one gets an self-consistent equation for A_0 : $A_0^{-2} \approx \frac{q^2 a_0^2}{\hbar^2} \frac{\tilde{m}^{(MB)}}{m} = \frac{q^2 a_0^2}{\hbar^2} \left(1 + \frac{Nq^2 A_0^2}{m\omega_c}\right)$, where the reduced Planck constant \hbar and lattice constant a is restored for clarity. The amplitude A_0 is experimentally determined by cavity size, *i.e.*, $A_0 = \sqrt{\frac{\hbar}{2\epsilon_r \epsilon_0 V \omega_c}}$ where ϵ_0 is the vacuum permittivity, ϵ_r is the relative permittivity, V is the volume of the cavity, and ω_c is the cavity frequency which can be controlled experimentally. One can then solve for the critical cavity length as shown in table I. For cavities with dimensions exceeding L_c , the system exhibits the CSL phase. It's also useful to check the lattice potential depth when the CSL phase appears, namely $\beta \approx 0.1$, which gives rise to results in table I.

From cavity photon-electron coupling to chiral interaction. To understand how the coupling to chiral cavity photons induces a CSL phase, it is pedagogical to derive the effective Hamiltonian of the system in terms of spins, particularly in the strong-coupling regime where the kinetic energy of electrons is much smaller compared to the interaction energy. This regime can be analyzed through the t/U expansion [56–58] of the Hubbard model eq. (6) at half-filling. This technique allows us to derive an effective spin Hamiltonian that captures the low-energy physics of the system. Notably, the chiral cavity introduces nontrivial phase factors in the hopping terms of the effective Hamiltonian, leading to chiral three-spin interactions. These interactions are essential for breaking time-reversal symmetry and stabilizing the CSL phase.

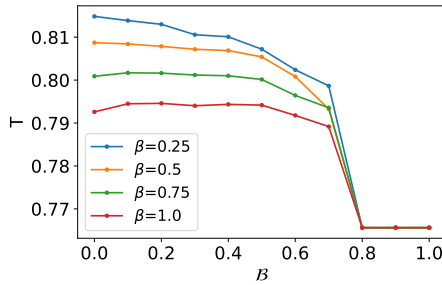


FIG. 4. Transmittance for waveguide coupled to the chiral cavity with kagome lattice inside. The transmittance approaches a constant with strong electron-photon interaction. All the simulations above are done with $t = 1$, $U' = 5$, $\omega_k = 1$ and $g = 0.1$.

In this limit, the effective Hamiltonian becomes:

$$H_{\text{eff}} = \sum_{\bullet\bullet} \frac{2|t_{ij}|^2}{U} (P_{ij} - 1) + \sum_{\bullet\bullet\bullet} \frac{6 \text{Im}(t_{ij} t_{jk} t_{ki})}{U^2} i(P_{ijk} - h.c.) \quad (8)$$

where the site-dependent hoppings are $t_{ij} = te^{i\varphi_{ij}}$, the first term describes Heisenberg-like interactions between neighboring spins, $P_{ij} - 1 = 2\mathbf{S}_i \cdot \mathbf{S}_j - \frac{1}{2}$, and the second term introduces a chiral three-spin interaction which is summed over all the triangles in the kagome lattice. The chiral nature of these terms stems from the nontrivial phase factors induced by the cavity mode, leading to the spin chirality operator: $i(P_{ijk} - h.c.) = -4\mathbf{S}_i \cdot \mathbf{S}_j \times \mathbf{S}_k$ which promotes a net spin current around triangular plaquettes of the kagome lattice.

This effective spin model reveals the crucial role of the phase factor induced by the chiral cavity field in generating chiral spin correlations. Both theoretical work [26, 59–61] and experimental evidence [62, 63] have shown that such chiral interactions are essential for stabilizing a CSL phase. While previous proposals suggest that the CSL phase can be experimentally detected through edge currents, thermal Hall effect measurements, and other signatures of topological order, in the following, we show that, in a setup with a chiral cavity, the photon states offer an additional pathway to probe the chiral spin states.

Probe the photon and electron states with a waveguide. We now return to the effective model eq. (6) in the AD frame to analyze experimental observables, focusing on the average photon number in the cavity and the associated transport properties when the system is coupled to a waveguide (see fig. 1). These quantities provide insight into the emergent quantum state of the system induced cavity quantum fluctuations. The averaged photon number $\bar{N} = \langle g | a^\dagger a | g \rangle$, where $|g\rangle$ is the ground state of the system in the lab frame, can be evaluated in the AD frame as: $\bar{N} = \langle 0 | \frac{1}{2} \xi^2 \mathbf{p}^2 | 0 \rangle$, where $|0\rangle$ is the ground state

in the AD frame, indicating that the photon number is proportional to the averaged kinetic energy of the electronic state. This observation directly links the quantum state of the cavity photons to the electronic structure of the kagome lattice in a chiral cavity.

Next, we examine the transport properties of photons through the waveguide coupled to the chiral cavity. The Hamiltonian governing photons in the cavity and in the waveguide is

$$H_0 = \omega_c a^\dagger a + \omega_k b_k^\dagger b_k \quad (9)$$

where ω_c is the cavity frequency, and ω_k is the frequency of photons in an external waveguide of mode k . The coupling between the cavity photons and the waveguide photons may be described by

$$H_g = g_k a^\dagger b_k + g_k^* b_k^\dagger a \quad (10)$$

In the AD frame, the coupling Hamiltonian becomes:

$$H_g^{(AD)} = g_k a^\dagger b_k + g_k^* b_k^\dagger a - g_k \xi \mathbf{p} \cdot \boldsymbol{\epsilon} b_k - g_k^* \xi \mathbf{p} \cdot \boldsymbol{\epsilon}^* b_k^\dagger. \quad (11)$$

This modified Hamiltonian reflects how the photon-electron interaction affects the transport of photons between the cavity and the external waveguide. The additional terms proportional to $\xi \mathbf{p}$ represent the influence of the electrons' momentum on the photon coupling. These terms induce a mixing between the cavity photons and the waveguide photons, mediated by the electron motion, and are responsible for modifying the transmittance of photons through the system.

The transmission amplitude can be calculated as [54]:

$$\begin{aligned} t_k &= \langle g, k, t = +\infty | S | g, k, t = -\infty \rangle \\ &= 1 - \frac{1}{2} \omega_k |g_k|^2 - (\omega_k + \frac{1}{2}) |g_k|^2 \langle 0 | \frac{1}{2} \xi^2 \mathbf{p}^2 | 0 \rangle \\ &= 1 - \frac{1}{2} \omega_k |g_k|^2 - (\omega_k + \frac{1}{2}) |g_k|^2 \bar{N} \end{aligned} \quad (12)$$

where $S = \mathcal{T} e^{-i \int dt (H_0 + H_g \delta(t))}$, $\xi = \frac{g A_0}{m \bar{\omega}_c}$, g_k is the coupling of the cavity and the waveguide, and ω_k is the dispersion of the waveguide. The corresponding transmittance T_k is given by $T_k = |t_k|^2$. This equation shows how the transmission of photons through the system is reduced due to the interaction between the photons and the electrons in the kagome lattice. The reduction in transmission is proportional to the photon-electron coupling g_k and the averaged photon number \bar{N} . This means that by measuring the transmittance, one can indirectly observe how the electron-photon interaction affects the electronic structure of the system. Particularly in the kagome lattice coupled to the chiral cavity case, we show the DMRG results of the transmittance in fig. 4. When the electron-photon coupling is weak, namely the system is in a CSL state, the effective gauge field makes the transmittance T_k a function of electron-photon coupling, while with strong electron-photon interaction, polarized spin state is insensitive to the gauge field leaving a

constant transmittance. In experimental setups, this observable provides a key signal of how the electronic state alters transport properties.

Discussion and Summary. This study demonstrates how coupling a kagome lattice to a chiral cavity field can realize a CSL phase, providing both a theoretical foundation and practical insights for tuning quantum materials using cQED. By leveraging the interplay between the frustrated geometry of the kagome lattice and cavity-induced chiral interactions, we show how the effective spin model at half-filling leads to the emergence of CSLs. We also discuss the experimental feasibility, highlighting recent cQED advances that enable the creation of tunable chiral cavities. Platforms such as kagome-based quantum magnets or ultracold atomic lattices in optical cavities offer promising avenues for realizing the predicted CSL phase. Experimental observables, including photon number and transport, provide clear signatures for detecting and manipulating CSL states in strongly correlated systems, opening new possibilities for their exploration and control.

Looking forward, this work opens several intriguing research directions. One of the most exciting possibilities is the study of doped CSLs, where the system is not restricted to half-filling. In such cases, the introduction of charge carriers could couple the charge degrees of freedom to the CSL state, potentially leading to new and exotic quantum phases. Doping a CSL can also break spin-charge separation, resulting in rich phase diagrams that may include superconducting phases or charge-density wave states. Studies in this context, such as those investigating fractionalized Fermi liquids and other strongly correlated doped CSLs, suggest that novel topological states could emerge from the interplay between charge fluctuations and spin chirality [64, 65].

In conclusion, the results presented here establish a solid framework for designing and probing CSLs within a practical chiral cavity setup, paving the way for further exploration of doped CSLs, cavity-tuned phase transitions, and nonequilibrium quantum phases in strongly correlated systems. Building on recent experimental advances in cavity-based setups [31, 33, 53], the intrinsic flexibility of cQED allows for precise control over interaction strengths and cavity parameters, enabling the engineering of phase transitions between various topological quantum phases. This approach also opens the possibility of harnessing cavity quantum fluctuations to create exotic excitations with fractional statistics, a crucial step toward advancing topological quantum computing.

uid state of the Heisenberg antiferromagnet, *Phys. Rev. B* **39**, 11879 (1989).

- [3] X. G. Wen, F. Wilczek, and A. Zee, Chiral spin states and superconductivity, *Phys. Rev. B* **39**, 11413 (1989).
- [4] W.-J. Hu, S.-S. Gong, and D. N. Sheng, Variational Monte Carlo study of chiral spin liquid in quantum antiferromagnet on the triangular lattice, *Phys. Rev. B* **94**, 075131 (2016).
- [5] Y. Huang, X.-Y. Dong, D. N. Sheng, and C. S. Ting, Quantum phase diagram and chiral spin liquid in the extended spin- $\frac{1}{2}$ honeycomb XY model, *Phys. Rev. B* **103**, L041108 (2021).
- [6] Y.-H. Zhang, D. N. Sheng, and A. Vishwanath, $SU(4)$ chiral spin liquid, exciton supersolid, and electric detection in Moiré bilayers, *Phys. Rev. Lett.* **127**, 247701 (2021).
- [7] T. A. Sedrakyan and A. V. Chubukov, Fermionic propagators for two-dimensional systems with singular interactions, *Phys. Rev. B* **79**, 115129 (2009).
- [8] T. A. Sedrakyan, A. Kamenev, and L. I. Glazman, Composite fermion state of spin-orbit-coupled bosons, *Phys. Rev. A* **86**, 063639 (2012).
- [9] T. A. Sedrakyan, L. I. Glazman, and A. Kamenev, Absence of bose condensation on lattices with moat bands, *Phys. Rev. B* **89**, 201112 (2014).
- [10] T. A. Sedrakyan, V. M. Galitski, and A. Kamenev, Statistical transmutation in floquet driven optical lattices, *Phys. Rev. Lett.* **115**, 195301 (2015).
- [11] T. A. Sedrakyan, L. I. Glazman, and A. Kamenev, Spontaneous formation of a nonuniform chiral spin liquid in a moat-band lattice, *Phys. Rev. Lett.* **114**, 037203 (2015).
- [12] R. Wang, B. Wang, and T. A. Sedrakyan, Chern-simons fermionization approach to two-dimensional quantum magnets: Implications for antiferromagnetic magnons and unconventional quantum phase transitions, *Phys. Rev. B* **98**, 064402 (2018).
- [13] S. Maiti and T. Sedrakyan, Fermionization of bosons in a flat band, *Phys. Rev. B* **99**, 174418 (2019).
- [14] R. Wang, Z. Y. Xie, B. Wang, and T. Sedrakyan, Emergent topological orders and phase transitions in lattice chern-simons theory of quantum magnets, *Phys. Rev. B* **106**, L121117 (2022).
- [15] C. Wei and T. A. Sedrakyan, Chiral spin liquid state of strongly interacting bosons with a moat dispersion: A monte carlo simulation, *Annals of Physics* **456**, 169354 (2023).
- [16] R. Wang, T. A. Sedrakyan, B. Wang, L. Du, and R.-R. Du, Excitonic topological order in imbalanced electron-hole bilayers, *Nature* **619**, 57 (2023).
- [17] C. Wei, V. V. Mkhitarian, and T. A. Sedrakyan, Unveiling chiral phases: Finite-size scaling as a probe of quantum phase transition in symmetry-enriched $c = 1$ conformal field theories (2024), *arXiv:2312.16660 [cond-mat.str-el]*.
- [18] S. Banerjee, W. Zhu, and S.-Z. Lin, Electromagnetic signatures of a chiral quantum spin liquid, *npj Quantum Materials* **8**, 63 (2023).
- [19] S. Sachdev, Kagome'- and triangular-lattice Heisenberg antiferromagnets: Ordering from quantum fluctuations and quantum-disordered ground states with unconfined bosonic spinons, *Phys. Rev. B* **45**, 12377 (1992).
- [20] X. Zhang, R. Jiang, X. Shen, X. Huang, Q.-D. Jiang, and W. Ku, Geometric inhibition of superflow in single-layer graphene suggests a staggered-flux superconductivity in bilayer and trilayer graphene, *Nano Letters* **24**, 10451

* qingdong.jiang@sjtu.edu.cn

- [1] V. Kalmeyer and R. B. Laughlin, Equivalence of the resonating-valence-bond and fractional quantum Hall states, *Phys. Rev. Lett.* **59**, 2095 (1987).
- [2] V. Kalmeyer and R. B. Laughlin, Theory of the spin liq-

(2024).

[21] D. L. Bergman, C. Wu, and L. Balents, Band touching from real-space topology in frustrated hopping models, *Physical Review B* **78**, 125104 (2008).

[22] G.-B. Jo, J. Guzman, C. K. Thomas, P. Hosur, A. Vishwanath, and D. M. Stamper-Kurn, Ultracold atoms in a tunable optical kagome lattice, *Phys. Rev. Lett.* **108**, 045305 (2012).

[23] C. Wei and T. A. Sedrakyan, Optical lattice platform for the Sachdev-Ye-Kitaev model, *Phys. Rev. A* **103**, 013323 (2021).

[24] C. Wei and T. A. Sedrakyan, Strange metal phase of disordered magic-angle twisted bilayer graphene at low temperatures: From flat bands to weakly coupled Sachdev-Ye-Kitaev bundles, *Phys. Rev. B* **108**, 064202 (2023).

[25] S.-S. Gong, W. Zhu, and D. N. Sheng, Emergent chiral spin liquid: Fractional quantum Hall effect in a kagome Heisenberg model, *Sci Rep* **4**, 6317 (2014).

[26] B. Bauer, L. Cincio, B. P. Keller, M. Dolfi, G. Vidal, S. Trebst, and A. W. W. Ludwig, Chiral spin liquid and emergent anyons in a kagome lattice Mott insulator, *Nature Communications* **5**, 5137 (2014).

[27] T.-H. Han, M. R. Norman, J.-J. Wen, J. A. Rodriguez-Rivera, J. S. Helton, C. Broholm, and Y. S. Lee, Correlated impurities and intrinsic spin-liquid physics in the kagome material herbertsmithite, *Phys. Rev. B* **94**, 060409 (2016).

[28] B.-Y. Sun, N. Goldman, M. Aidelsburger, and M. Bükov, Engineering and probing non-abelian chiral spin liquids using periodically driven ultracold atoms, *PRX Quantum* **4**, 020329 (2023).

[29] C. Kuhlenkamp, W. Kadow, A. m. c. Imamoğlu, and M. Knap, Chiral pseudospin liquids in moiré heterostructures, *Phys. Rev. X* **14**, 021013 (2024).

[30] M. Kiffner, J. R. Coulthard, F. Schlawin, A. Ardavan, and D. Jaksch, Manipulating quantum materials with quantum light, *Phys. Rev. B* **99**, 085116 (2019).

[31] F. Schlawin, D. M. Kennes, and M. A. Sentef, Cavity quantum materials, *Applied Physics Reviews* **9**, 011312 (2022), https://pubs.aip.org/aip/apr/article-pdf/doi/10.1063/5.0083825/19819541/011312_1_online.pdf.

[32] Z. Guo and Z. Cai, Vacuum induced three-body delocalization in cavity quantum materials (2024), [arXiv:2407.15032 \[cond-mat.dis-nn\]](https://arxiv.org/abs/2407.15032).

[33] A. Chiocchetta, D. Kiese, C. P. Zelle, F. Piazza, and S. Diehl, Cavity-induced quantum spin liquids, *Nature Communications* **12**, 5901 (2021).

[34] T. Espinosa-Ortega, O. Kyriienko, O. V. Kibis, and I. A. Shelykh, Semiconductor cavity QED: Band gap induced by vacuum fluctuations, *Phys. Rev. A* **89**, 062115 (2014).

[35] E. Plum and N. I. Zheludev, Chiral mirrors, *Applied Physics Letters* **106**, 221901 (2015), https://pubs.aip.org/aip/apl/article-pdf/doi/10.1063/1.4921969/14315841/221901_1_online.pdf.

[36] C. Schäfer, M. Ruggenthaler, and A. Rubio, Ab initio nonrelativistic quantum electrodynamics: Bridging quantum chemistry and quantum optics from weak to strong coupling, *Phys. Rev. A* **98**, 043801 (2018).

[37] X. Wang, E. Ronca, and M. A. Sentef, Cavity quantum electrodynamical Chern insulator: Towards light-induced quantized anomalous Hall effect in graphene, *Phys. Rev. B* **99**, 235156 (2019).

[38] Q.-D. Jiang and F. Wilczek, Quantum atmospherics for materials diagnosis, *Phys. Rev. B* **99**, 201104 (2019).

[39] D. G. Baranov, B. Munkhbat, N. O. Länk, R. Verre, M. Käll, and T. Shegai, Circular dichroism mode splitting and bounds to its enhancement with cavity-plasmon-polaritons, *Nanophotonics* **9**, 283 (2020).

[40] D. G. Baranov, B. Munkhbat, E. Zhukova, A. Bisht, A. Canales, B. Rousseaux, G. Johansson, T. J. Antosiewicz, and T. Shegai, Ultrastrong coupling between nanoparticle plasmons and cavity photons at ambient conditions, *Nature Communications* **11**, 2715 (2020).

[41] J. C. Owens, M. G. Panetta, B. Saxberg, G. Roberts, S. Chakram, R. Ma, A. Vrajitoarea, J. Simon, and D. I. Schuster, Chiral cavity quantum electrodynamics, *Nature Physics* **18**, 1048 (2022).

[42] J. Bloch, A. Cavalleri, V. Galitski, M. Hafezi, and A. Rubio, Strongly correlated electron–photon systems, *Nature* **606**, 41 (2022).

[43] C. Valagianopoulos, Electromagnetic analog to magic angles in twisted bilayers of two-dimensional media, *Phys. Rev. Appl.* **18**, 044011 (2022).

[44] K. Zhu, Z. Yang, Q.-D. Jiang, Z. Chai, Z. Li, Z. Zhao, Y. Wang, F. Shi, C.-K. Duan, and X. Rong, Experimental sensing quantum atmosphere of a single spin, *Quantum Frontiers* **3**, 1 (2024).

[45] L. Yang and Q.-D. Jiang, Emergent haldane model and photon-valley locking in chiral cavities (2024), [arXiv:2403.11063 \[cond-mat.mes-hall\]](https://arxiv.org/abs/2403.11063).

[46] C. Jiang, M. Baggio, and Q.-D. Jiang, Engineering flat bands in twisted-bilayer graphene away from the magic angle with chiral optical cavities, *Physical Review Letters* **132**, 10.1103/physrevlett.132.166901 (2024).

[47] H. Hübener, U. De Giovannini, C. Schäfer, J. Andberger, M. Ruggenthaler, J. Faist, and A. Rubio, Engineering quantum materials with chiral optical cavities, *Nature materials* **20**, 438 (2021).

[48] K. Voronin, A. S. Taradin, M. V. Gorkunov, and D. G. Baranov, Single-handedness chiral optical cavities, *ACS Photonics* **9**, 2652 (2022).

[49] D. G. Baranov, C. Schäfer, and M. V. Gorkunov, Toward molecular chiral polaritons, *ACS Photonics* (2023).

[50] G. Jarc, S. Y. Mathengattil, A. Montanaro, F. Giusti, E. M. Rigoni, R. Sergo, F. Fassoli, S. Winnerl, S. Dal Zilio, D. Mihailovic, P. Prelovšek, M. Eckstein, and D. Fausti, Cavity-mediated thermal control of metal-to-insulator transition in 1T-TaS₂, *Nature* **622**, 487 (2023).

[51] E. Viñas Boström, A. Sriram, M. Claassen, and A. Rubio, Controlling the magnetic state of the proximate quantum spin liquid α -RuCl₃ with an optical cavity, *npj Computational Materials* **9**, 202 (2023).

[52] A. Belov, Y. E. Lozovik, and V. Pokrovskii, Lamb shift of Rydberg atoms in a cavity, *Zh. Eksp. Teor. Fiz.* **96**, 560 (1989).

[53] Y. Ashida, A. m. c. İmamoğlu, and E. Demler, Cavity quantum electrodynamics at arbitrary light-matter coupling strengths, *Phys. Rev. Lett.* **126**, 153603 (2021).

[54] See Supplemental Material at [URL will be inserted by publisher] for detailed derivations.

[55] C. Hubig, I. P. McCulloch, U. Schollwöck, and F. A. Wolf, Strictly single-site DMRG algorithm with subspace expansion, *Phys. Rev. B* **91**, 155115 (2015).

[56] M. Takahashi, Half-filled Hubbard model at low temperature, *Journal of Physics C: Solid State Physics* **10**, 1289 (1977).

[57] A. H. MacDonald, S. M. Girvin, and D. Yoshioka, $\frac{t}{U}$ expansion for the Hubbard model, *Phys. Rev. B* **37**, 9753 (1988).

[58] O. I. Motrunich, Orbital magnetic field effects in spin

liquid with spinon Fermi sea: Possible application to κ -(ET)₂Cu₂(CN)₃, *Phys. Rev. B* **73**, 155115 (2006).

[59] B. Bauer, B. P. Keller, M. Dolfi, S. Trebst, and A. W. W. Ludwig, Gapped and gapless spin liquid phases on the kagome lattice from chiral three-spin interactions (2014), [arXiv:1303.6963 \[cond-mat.str-el\]](https://arxiv.org/abs/1303.6963).

[60] K. Kumar, K. Sun, and E. Fradkin, Chiral spin liquids on the kagome lattice, *Phys. Rev. B* **92**, 094433 (2015).

[61] S. Niu, J. Hasik, J.-Y. Chen, and D. Poilblanc, Chiral spin liquids on the kagome lattice with projected entangled simplex states, *Phys. Rev. B* **106**, 245119 (2022).

[62] M. Claassen, H.-C. Jiang, B. Moritz, and T. P. Devreux, Dynamical time-reversal symmetry breaking and photo-induced chiral spin liquids in frustrated Mott insulators, *Nature Communications* **8**, 1192 (2017).

[63] W. Schweika, M. Valldor, J. D. Reim, and U. K. Rößler, Chiral spin liquid ground state in YBaCo₃FeO₇, *Phys. Rev. X* **12**, 021029 (2022).

[64] T. Grover, N. Trivedi, T. Senthil, and P. A. Lee, Weak Mott insulators on the triangular lattice: Possibility of a gapless nematic quantum spin liquid, *Phys. Rev. B* **81**, 245121 (2010).

[65] L. Savary, J. Ruhman, J. W. F. Venderbos, L. Fu, and P. A. Lee, Superconductivity in three-dimensional spin-orbit coupled semimetals, *Phys. Rev. B* **96**, 214514 (2017).

Supplemental Material for Cavity-Vacuum-Induced Chiral Spin Liquids in Kagome Lattices: Tuning and Probing Topological Quantum Phases via Cavity Quantum Electrodynamics

Chenan Wei,^{1,2} Liu Yang,^{3,4} and Qing-Dong Jiang^{3,4,5}

¹*Department of Physics, University of Massachusetts, Amherst, Massachusetts 01003, USA*

²*Department of Physics, University of Alberta, Edmonton, Alberta T6G 2E1, Canada*

³*Tsung-Dao Lee Institute, Shanghai Jiao Tong University, Shanghai 200240, China*

⁴*School of Physics and Astronomy, Shanghai Jiao Tong University, Shanghai 200240, China*

⁵*Shanghai Branch, Hefei National Laboratory, Shanghai 201315, China*

(Dated: November 12, 2024)

In this supplemental material, we will present the detailed derivation of the equations used in the main text.

I. KAGOME LATTICE COUPLED TO A CHIRAL CAVITY IN THE ASYMPTOTIC DECOUPLED FRAME

A. A single particle version

We start with the Hamiltonian describing electrons in a kagome lattice coupled to a single-mode chiral cavity presented in the main text

$$H = \frac{(\boldsymbol{\sigma} \cdot (\mathbf{p} - q\mathbf{A}))^2}{2m} + V_{\text{lattice}}(\mathbf{r}) + \omega_c a^\dagger a, \quad (1)$$

where $\boldsymbol{\sigma}$ is the vector of Pauli matrices, \mathbf{p} is the momentum of the electrons, m is the mass of the electrons, the vector potential is $\mathbf{A} = A_0(\boldsymbol{\epsilon}a + \boldsymbol{\epsilon}^*a^\dagger)$ and $\boldsymbol{\epsilon} = \frac{1}{\sqrt{2}}(1, i)$, which is circularly polarized because of the chiral cavity, a and a^\dagger are photon annihilation and creation operators.

To simplify the Hamiltonian 1, the following two relations can be used

$$(\boldsymbol{\sigma} \cdot \mathbf{a})(\boldsymbol{\sigma} \cdot \mathbf{b}) = \mathbf{a} \cdot \mathbf{b} + i\boldsymbol{\sigma} \cdot (\mathbf{a} \times \mathbf{b}), \quad (2)$$

and

$$[A_x, A_y] = -iA_0^2. \quad (3)$$

With the above relations, one can expand the Hamiltonian 1 and gets

$$H = \frac{\mathbf{p}^2}{2m} - \frac{q\mathbf{p} \cdot \mathbf{A}}{m} - \frac{q\boldsymbol{\sigma} \cdot \mathbf{B}}{2m} + V_{\text{lattice}}(\mathbf{r}) + \tilde{\omega}_c a^\dagger a + \frac{q^2 A_0^2 \sigma_z}{2m}, \quad (4)$$

where $\tilde{\omega}_c = \omega_c + \frac{q^2 A_0^2}{m}$, and $\mathbf{B} = \partial_x A_y - \partial_y A_x$. If we consider the system at the peak of the vector potential \mathbf{A} , the magnetic field vanishes and hence we can remove the term $-\frac{q\boldsymbol{\sigma} \cdot \mathbf{B}}{2m}$.

To decouple the cavity photons from the electronic degrees of freedom, the asymptotically decoupled(AD) transformation is employed, which is a unitary transformation

$$U = \exp(-i\xi \mathbf{p} \cdot \boldsymbol{\pi}) \quad (5)$$

where the parameter $\xi = \frac{qA_0}{m\tilde{\omega}_c}$ is chosen such that the coupling between the electron and photon vanishes, and $\boldsymbol{\pi} = i(\boldsymbol{\epsilon}^* a^\dagger - \boldsymbol{\epsilon} a)$ represents the photon field momentum.

To calculate the transformed Hamiltonian

$$H_U = U^\dagger H U = \exp(i\xi \mathbf{p} \cdot \boldsymbol{\pi}) H \exp(-i\xi \mathbf{p} \cdot \boldsymbol{\pi}), \quad (6)$$

the Hadamard formula is used

$$e^{\hat{A}} \hat{B} e^{-\hat{A}} = \hat{B} + [\hat{A}, \hat{B}] + \frac{1}{2!} [\hat{A}, [\hat{A}, \hat{B}]] + \frac{1}{3!} [\hat{A}, [\hat{A}, [\hat{A}, \hat{B}]]] + \dots \quad (7)$$

One can verify that, under the AD transformation

$$U^\dagger \mathbf{A} U = A_0 [\boldsymbol{\epsilon}^* a^\dagger + \boldsymbol{\epsilon} a + \xi(\mathbf{p} \cdot \boldsymbol{\epsilon}^*) \boldsymbol{\epsilon} + \xi(\mathbf{p} \cdot \boldsymbol{\epsilon}) \boldsymbol{\epsilon}^*], \quad (8)$$

$$U^\dagger a^\dagger a U = a^\dagger a + \xi \mathbf{p} \cdot (\boldsymbol{\epsilon}^* a^\dagger + \boldsymbol{\epsilon} a) + \xi^2 (\mathbf{p} \cdot \boldsymbol{\epsilon}) (\mathbf{p} \cdot \boldsymbol{\epsilon}^*) \quad (9)$$

$$U^\dagger \mathbf{r} U = \mathbf{r} + \xi \boldsymbol{\pi} - \frac{1}{2} \xi^2 \mathbf{p} \times \hat{\mathbf{z}}. \quad (10)$$

With the above equations, the transformed Hamiltonian, under the photon vacuum subspace, turns out to be

$$\langle 0 | H_U | 0 \rangle \approx \frac{\mathbf{p}^2}{2\tilde{m}} + V_{\text{lattice}}(\mathbf{r} - \frac{1}{2} \xi^2 \mathbf{p} \times \hat{\mathbf{z}}) + \frac{q^2 A_0^2 \sigma_z}{2m} \quad (11)$$

where $\frac{1}{\tilde{m}} = \frac{1}{m} (1 - \frac{q^2 A_0^2}{m \tilde{\omega}_c})$, namely $\tilde{m} = m + \frac{q^2 A_0^2}{\omega_c}$.

The lattice potential can be further simplified

$$V_{\text{lattice}}(\mathbf{r} - \frac{1}{2} \xi^2 \mathbf{p} \times \hat{\mathbf{z}}) \approx V_{\text{lattice}}(\mathbf{r}) - \frac{1}{2} \xi^2 \mathbf{p} \cdot (\hat{\mathbf{z}} \times \nabla V_{\text{lattice}}(\mathbf{r})). \quad (12)$$

The second term works as an effective gauge field

$$\mathbf{A}_{\text{eff}} = \frac{\tilde{m} \xi^2}{2} \hat{\mathbf{z}} \times \nabla V_{\text{lattice}}(\mathbf{r}). \quad (13)$$

As a result, the Hamiltonian in AD frame becomes

$$H_U = \frac{(\mathbf{p} - q\mathbf{A}_{\text{eff}})^2}{2\tilde{m}} + V_{\text{eff}}(\mathbf{r}) + \frac{q^2 A_0^2 \sigma_z}{2m}, \quad (14)$$

where the effective potential

$$V_{\text{eff}}(\mathbf{r}) = V_{\text{lattice}}(\mathbf{r}) - \frac{\tilde{m}\xi^4}{8}(\nabla V_{\text{lattice}}(\mathbf{r}))^2. \quad (15)$$

With these preparation, one can straightforwardly write down the lattice model in the AD frame

$$H_{\text{AD}} = - \sum_{\langle i,j \rangle, \sigma} t e^{i\varphi_{ij}} c_{i\sigma}^\dagger c_{j\sigma} + U' \sum_i n_{i\uparrow} n_{i\downarrow} + \sum_i \frac{q^2 A_0^2 \sigma_z}{2m} (n_{i\uparrow} - n_{i\downarrow}) \quad (16)$$

as presented in the main text. The phase factor can be computed from the effective gauge field $\varphi_{ij} = q \int_{\mathbf{r}_i}^{\mathbf{r}_j} \mathbf{A}_{\text{eff}} \cdot d\mathbf{r}$.

B. A many-body version

Now, if we consider the mediated interaction between electrons, we can derive the AD Hamiltonian from a many-body perspective. We now write down the Hamiltonian for all the electrons as follows:

$$\mathcal{H} = \sum_{j=1}^N \left(\frac{\mathbf{p}_j^2}{2m} - \frac{q\mathbf{p}_j \cdot \mathbf{A}}{m} + V_{\text{lattice}}(\mathbf{r}_j) + \frac{q^2 A_0^2 \sigma_z^j}{2m} \right) + \omega_c (a^\dagger a + \frac{1}{2}), \quad (17)$$

where we have removed the interaction $\sigma \cdot \mathbf{B}$ by considering the material layer at the peak of the vector potential. Now we apply the unitary transformation

$$\mathcal{U} = \exp \left[-i\xi \left(\sum_j \mathbf{p}_j \right) \cdot \hat{\boldsymbol{\pi}} \right], \quad (18)$$

where

$$\xi = \frac{qA_0}{m\tilde{\omega}_c^{(MB)}}, \quad (19)$$

with

$$\tilde{\omega}_c^{(MB)} = \omega_c \left(1 + \frac{Nq^2 A_0^2}{m\omega_c} \right), \quad (20)$$

to the many-body Hamiltonian and obtain

$$\begin{aligned} \mathcal{H}_U &= \mathcal{U}^\dagger \mathcal{H} \mathcal{U} \\ &= \left[\sum_{j=1}^N \frac{\mathbf{p}_j^2}{2m} + V_{\text{lattice}}(\mathbf{r}_j + \boldsymbol{\tau}_j) + \frac{q^2 A_0^2 \sigma_z^j}{2m} \right] - \frac{\tilde{\omega}_c^{(MB)}}{2} \left(\sum_{j=1}^N \xi \mathbf{p}_j \right)^2 + \tilde{\omega}_c^{(MB)} (a^\dagger a + \frac{1}{2}). \end{aligned} \quad (21)$$

Here, we define a new operator $\boldsymbol{\tau}_j$ as

$$\boldsymbol{\tau}_j = \xi \hat{\boldsymbol{\pi}} - \frac{1}{2} \xi^2 \mathbf{p}_j \times \hat{\mathbf{z}}. \quad (22)$$

The term

$$\mathcal{H}' = -\frac{\tilde{\omega}_c^{(MB)}}{2} \left(\sum_{j=1}^N \xi \mathbf{p}_j \right)^2 \quad (23)$$

contains an all-to-all interaction. In fact, the all-to-all cavity-mediated interaction can be reduced to an electron-independent Hamiltonian because the system is uniform on a large scale [1]. Specifically, every particle experiences an identical average effect from the rest, effectively averaging out the microscopic interactions. To perform the electron-independent approximation, we first take the expectation of \mathcal{H}' under a many-body wave function as follow $\Psi(x_1, \dots, x_N)$:

$$\mathcal{H}'[\Psi] = -\frac{\tilde{\omega}_c^{(MB)} \xi^2}{2} \int d\Gamma \Psi^*(x) \left(\sum_{j=1}^N \mathbf{p}_j \right)^2 \Psi(x), \quad (24)$$

Here the integrated variable $d\Gamma = \Pi_i dx_i$. Now, we introduce the single-body and two-body wave functions $\Psi_1(x)$ and $\Psi_2(x_1, x_2)$ that satisfy

$$\Psi_1^*(x_1) \Psi_1(x_1) = \int dx_2 dx_3 \dots dx_N \Psi^*(x_1, \dots, x_N) \Psi(x_1, \dots, x_N), \quad (25)$$

$$\Psi_2^*(x_1, x_2) \Psi_2(x_1, x_2) = \int dx_3 \dots dx_N \Psi^*(x_1, \dots, x_N) \Psi(x_1, \dots, x_N). \quad (26)$$

Now, we apply the electron-independent approximation assuming the two-body wave function Ψ_2 as follow

$$\Psi_2(x_1, x_2) = \Psi_1(x_1 + x_2) \chi(x_1 - x_2) \approx \Psi_1(x_1 + x_2). \quad (27)$$

Then, we obtain

$$\mathcal{H}'[\Psi_1] = -\frac{1}{2m} \frac{Nq^2 A_0^2}{m \tilde{\omega}_c^{(MB)}} \int dx \Psi_1^*(x) (-i\nabla)^2 \Psi_1(x). \quad (28)$$

Combing this energy term with other terms in the Hamiltonian, we have

$$\langle 0 | H_U | 0 \rangle \approx \sum_{j=1}^N \frac{\mathbf{p}_j^2}{2\tilde{m}^{(MB)}} + V_{\text{lattice}}(\mathbf{r}_j - \frac{1}{2} \xi^2 \mathbf{p}_j \times \hat{\mathbf{z}}) + \frac{q^2 A_0^2 \sigma_z^j}{2m}, \quad (29)$$

$$\tilde{m}^{(MB)} = m \left(1 + \frac{Nq^2 A_0^2}{m \omega_c} \right). \quad (30)$$

This Hamiltonian has been derived in Ref. [1]. Following the same steps as we did in the single particle case, the eq. (29) leads to the same form of effective-gauge-field-coupled Hamiltonian eq. (14) with a substitution

$$\begin{aligned} \tilde{\omega}_c &\rightarrow \tilde{\omega}_c^{(MB)}, \\ \tilde{m} &\rightarrow \tilde{m}^{(MB)}. \end{aligned} \quad (31)$$

II. PHOTON STATE IN THE CHIRAL CAVITY WITH KAGOME LATTICE INSIDE

We start by computing the averaged photon number $\bar{N} = \langle g| a^\dagger a |g\rangle$, where $|g\rangle$ is the ground state of the system in the lab frame

$$\begin{aligned}\bar{N} &= \langle g| UU^\dagger a^\dagger a UU^\dagger |g\rangle \\ &= \langle 0| a^\dagger a + \xi \mathbf{p} \cdot (\epsilon^* a^\dagger + \epsilon a) + \xi^2 (\mathbf{p} \cdot \epsilon^*) (\mathbf{p} \cdot \epsilon) |0\rangle \\ &= \langle 0| \frac{1}{2} \xi^2 \mathbf{p}^2 |0\rangle.\end{aligned}\quad (32)$$

This shows that the photon number is proportional to the averaged kinetic energy of the electronic state discussed in the main text.

Next, we compute the transportation of photons through the waveguide coupled to the chiral cavity. As presented in the main text, the Hamiltonian of photons in the cavity and in the waveguide is

$$H_0 = \omega_c a^\dagger a + \omega_k b_k^\dagger b_k \quad (33)$$

where ω_c is the cavity frequency, and ω_k is the frequency of photons in the waveguide of wave number k . The coupling between the cavity photons and the waveguide photons is described by

$$H_g = g_k a^\dagger b_k + g_k^* b_k^\dagger a \quad (34)$$

In the AD frame, the coupling Hamiltonian becomes:

$$H_g^{(AD)} = g_k a^\dagger b_k + g_k^* b_k^\dagger a - g_k \xi \mathbf{p} \cdot \epsilon b_k - g_k^* \xi \mathbf{p} \cdot \epsilon^* b_k^\dagger. \quad (35)$$

The transmission amplitude can be calculated within the time dependent perturbation:

$$\begin{aligned}t_k &= \langle g, k, t = +\infty | \mathcal{T} e^{-i \int dt (H_0 + H_g \delta(t))} |g, k, t = -\infty \rangle \\ &\approx \langle g, k, t = +\infty | e^{-i H_0 t} \left[1 - i \int_{-\infty}^{+\infty} dt_1 V(t_1) - \int_{-\infty}^{+\infty} dt_1 \int_{-\infty}^{t_1} dt_2 V(t_1) V(t_2) \right] |g, k, t = -\infty \rangle\end{aligned}\quad (36)$$

where we have defined

$$V(t) = e^{itH_0} H_g \delta(t) e^{-itH_0}. \quad (37)$$

As before, it is easier to work in AD frame, and we compute t_k order by order. The zeroth order is trivially $t_k^{(0)} = 1$. The first order is $t_k^{(1)} = 0$ because of the annihilation operators acting on the zero photon state. The second order term is the first non-trivial term. To compute $t_k^{(2)}$, it would be helpful to first check the commutation relation

$$[H_0, H_g] = (\omega_c - \omega_k) g_k a^\dagger b_k - (\omega_c - \omega_k) g_k^* a b_k^\dagger \quad (38)$$

and hence

$$ad_{H_0}^n := \underbrace{[H_0, [H_0, \cdots [H_0, H_g]]]}_{nH_0} = (\omega_c - \omega_k)g_k a^\dagger b_k - (\omega_c - \omega_k)g_k^* a b_k^\dagger. \quad (39)$$

With this, the Hadamard formula leads to

$$\begin{aligned} V(t) &= e^{itH_0} H_g \delta(t) e^{-itH_0} \\ &= \sum_{n=0}^{\infty} \frac{(it)^n}{n!} ad_{H_0}^n H_g \delta(t) \\ &= g_k(t) a^\dagger b_k + g_k^*(t) a b_k^\dagger, \end{aligned} \quad (40)$$

where we have defined

$$g_k(t) = e^{it(\omega_c - \omega_k)} \delta(t) g_k. \quad (41)$$

Now the $t_k^{(2)}$ is ready to be computed

$$\begin{aligned} t_k^{(2)} &= - \int_{-\infty}^{+\infty} dt_1 \int_{-\infty}^{t_1} dt_2 \langle 0, k | U^\dagger V(t_1) U U^\dagger V(t_2) U | 0, k \rangle \\ &= - \int_{-\infty}^{+\infty} dt_1 \int_{-\infty}^{t_1} dt_2 \langle 0, k | g_k^*(t_1) g_k(t_2) \omega_k | 0, k \rangle \\ &\quad - \int_{-\infty}^{+\infty} dt_1 \int_{-\infty}^{t_1} dt_2 \langle 0, k | g_k(t_1) g_k^*(t_2) \xi^2 (\mathbf{p} \cdot \boldsymbol{\epsilon}) (\mathbf{p} \cdot \boldsymbol{\epsilon}^*) (1 + \omega_k) | 0, k \rangle \\ &\quad - \int_{-\infty}^{+\infty} dt_1 \int_{-\infty}^{t_1} dt_2 \langle 0, k | g_k^*(t_1) g_k(t_2) \xi^2 (\mathbf{p} \cdot \boldsymbol{\epsilon}^*) (\mathbf{p} \cdot \boldsymbol{\epsilon}) \omega_k | 0, k \rangle \\ &= -\frac{1}{2} \omega_k |g_k|^2 - (\omega_k + \frac{1}{2}) |g_k|^2 \langle 0 | \frac{1}{2} \xi^2 p^2 | 0 \rangle \\ &= -\frac{1}{2} \omega_k |g_k|^2 - (\omega_k + \frac{1}{2}) |g_k|^2 \bar{N} \end{aligned} \quad (42)$$

which, combining with the unity from the zeroth order, reproduces the formula we claimed in the main text.

[1] Y. Ashida, A. m. c. İmamoğlu, and E. Demler, Cavity quantum electrodynamics at arbitrary light-matter coupling strengths, [Phys. Rev. Lett. 126, 153603 \(2021\)](#).